J Polym Res (2015) 22: 152
DOI 10.1007/s10965-015-0797-0

ORIGINAL PAPER

Simultaneous electrochemical determination of dopamine, uric acid and ascorbic acid using silver nanoparticles deposited on polypyrrole nanofibers

Khadijeh Ghanbari[1] · **Nahid Hajheidari**[1]

Received: 11 November 2014 / Accepted: 10 July 2015 / Published online: 18 July 2015

Abstract Silver nanoparticles modified polypyrrole (PPy) nanofibers were fabricated and used for the simultaneous determination of ascorbic acid (AA), dopamine (DA) and uric acid (UA) with good selectivity and high sensitivity. Polypyrrole nanofibers were prepared through electrodeposition, while silver nanoparticles were deposited on PPy nanofiber by electrodeposition and electrochemical oxidation in situ. The morphology and structure of silver nanoparticles/polypyrrole nanocomposite (Ag/PPy) were characterized by scanning electron microscopy (SEM), X-ray diffraction (XRD) and Fourier transform infrared (FT-IR). Compared with the bare glassy carbon electrode (GCE) and PPy/GCE, Ag/PPy modified GCE (Ag-PPy/GCE) exhibited much higher electrocatalytic activities toward oxidation of AA, DA, and UA with increasing the peak currents and decreasing the oxidation overpotentials. Cyclic voltammetry (CV) results showed that DA, AA, and UA could be detected selectively and sensitively at Ag-PPy/GCE with peak-to-peak separation of 120 mV and 170 mV for AA-DA and DA-UA, respectively. The calibration curves for AA, DA, and UA were obtained in the range of 10–580 μM, 0.5–155 μM and 2–100 μM, respectively. The lowest detection limits (S/N= 3) were 1.8 μM, 0.1 μM, and 0.5 μM for AA, DA, and UA, respectively. With good selectivity and sensitivity, the present method was applied to determination of DA in injectable medicine and UA in urine sample.

Keywords Silver nanoparticles · Polypyrrole nanofiber · Ascorbic acid · Uric acid · Dopamine

✉ Khadijeh Ghanbari
kh_ghanb@yahoo.com; kh.ghanbari@alzahra.ac.ir

[1] Faculty of Physic Chemistry, Alzahra University, Vanak, Tehran 1993891167, Iran

Introduction

Ascorbic acid (AA) is a common anti-oxidant and plays an important role in prevention and treatment of some diseases such as scurvy, common cold, cancer, and hepatic diseases [1, 2]. Dopamine (DA) is a catecholamine neurotransmitter in the brain. Uncommon levels of DA may result in drastic neurological disorders such as Parkinson's disease and addiction [3–5]. Uric acid (UA) is the early product of purine metabolism and is present in biological fluids such as blood or urine [6]. Disturbance of UA is the symptom of various diseases such as hyperuricemia, gout, and pneumonia [7, 8].

So, it is of utmost importance to detect these species with desired sensitivity and accuracy. However, detection of these species in physiological samples is challenging because of the high concentrations of ascorbic acid (0.2–0.5 mM) accompanied with small concentrations of DA (10^{-8} to 10^{-7} M) in physiological samples [9–11].

Therefore, selective detection of DA, AA, and UA, and even their simultaneous detection in the presence of large amounts of AA have received tremendous attention in biomedical chemistry, as well as diagnostic and pathological research [12, 13] owing to their similar properties. Numerous methods have been developed for simultaneous determination of these species in biological fluids [14].

Whereas DA, AA, and UA are electrochemically active, electrochemical methods appear to be convenient for their simultaneous determination due to their high sensitivity, easy operation, cost effectiveness, and fast response [15, 16]. However, overlapping of the oxidation peaks of these three species is a main disadvantage of the electrochemical technique to homogeneous electron transfer at bare electrodes [17, 18]. So, selective detection of DA, UA, and AA in the presence of the other two species or their simultaneous

determination has been a basic goal in many studies in this field. To this end, various chemically modified electrodes have been prepared.

Numerous nanomaterials modified electrodes are ideal candidates to tackle the challenge of bioanalytical problems owing to their unique mechanical, physical, and chemical properties. Among them, metal nanoparticles (MNPs) modified electrodes have drawn particular attention due to their high surface area, effective mass transport, catalysis, and control over local microenvironment contrasted to macro-electrodes [19, 20].

Incorporating metal nanoparticles into polymer matrices is of interest in recent studies for many goals [21–24]. The polymer can be a matrix to stabilize formation of metal nanoparticles (MNPs) and to prevent the agglomeration process. The stabilized MNPs then can be studied for their catalytic, optical, magnetic, mechanical, and electrical properties. On the other hand, the MNPs can be deposited into polymer matrices to improve some properties of the polymer such as the Raman's activity and conductivity or to modify the polymer structures, as well as the electronic, mechanical, and electrical properties. The MNPs can also serve as fillers to modify the polymer surface morphology, or even to print nanoelectric circuit using some other templates or masks. Conducting polymers such as polypyrrole might lose their conductivity by time, while the MNPs fillers can be permanently conducting.

Silver nanoparticles have obtained increasing attention in the past decade due to their attractive electric [25, 26], optical [27, 28], catalytic [29, 30], and particularly antimicrobial properties [31, 32] that are well established and extensively investigated mainly in colloidal systems. Nevertheless, many practical applications of silver nanoparticles require their entrapment on different substrates and matrices [33–35]. From this point of view, polymers are the materials of the first choice because of their specific morphology, chemical and structural nature with long polymeric chains allowing incorporation and fine dispersion of nanoparticles.

In this work, we fabricated Ag/PPy nanocomposites on the surface of GCE by electrochemical deposition, and their morphology and crystal structures were investigated in some detail. The modified electrode was used for simultaneous determination of AA, DA and UA and showed perfect selectivity and excellent electrochemical activity towards the oxidation of AA, DA and UA. The detection of UA in urine sample and DA in injectable medicine was finally demonstrated as real sample applications.

Experimental

Instruments

The surface morphological characterization of Ag-PPy/GCE was examined by means of field emission scanning electron microscopy (FE-SEM) (Zeiss Sigma VP, Germany) at an accelerating voltage of 20 kV. The phase structures of the as-prepared samples were characterized by X-ray diffraction (XRD) (Model: X'Pert MPD, Company: Philips, Holland). FT-IR spectra (KBr pellets) were recorded using a (Model: Tensor 27, Company: Bruker) instrument. Electrochemical measurements were performed by an electrochemical system analyzer (Sama Instruments, Iran). A conventional three-electrode system was used, containing an Ag/AgCl/saturated KCl as reference electrode, a Pt wire as counter electrode, and a bare or modified glassy carbon electrode (GCE) as working electrode.

Materials

Ascorbic acid (AA), uric acid (UA), and dopamine (DA) was purchased from Sigma-Aldrich. Pyrrole, Acetic acid, silver nitrate, sodium hydroxide was obtained from Merck. All the other chemicals were of analytical grade and used as received. Pyrrole was distilled under vacuum and stored frozen. All the aqueous solutions were prepared with twice-distilled water.

Preparation of the modified electrodes

A bare GCE was polished successively with 0.05 μm alumina slurry on a synthetic cloth, rinsed with pure water, and sonicated subsequently in a 1:1 double distilled water and ethanol for 5 min. Before the polymerization, electrolyte solutions were desecrated thoroughly with pure nitrogen. Ag/PPy modified electrode was prepared by procedure has reported by reference [22]. In this method electrochemical deposition of PPy on GCE was performed at ambient temperature and potentiostatically 0.8 V vs. Ag/AgCl in aqueous solution containing 0.15 M pyrrole, 0.10 M $LiClO_4$ and 0.10 M carbonate. Freshly prepared PPy nanofibers electrodes were usually conditioned in 0.10 M $HClO_4$ solution for 24 h to remove the carbonate ions.

The PPy nanofibers modified electrode was treated at 0.85 V for 300 s in 0.15 M NaOH solution. The silver nanoparticles were then electrochemically deposited on the prepared PPy nanofiber in aqueous solution containing 1.0 mM $AgNO_3$ and 0.1 M $NaNO_3$ by a double pulse technique. The double pulse technique involves applying of two pulses; the first, the nucleation pulse E_1 and the second, the growth pulse, E_2. The pulse parameters were chosen carefully to avoid degrading the polymer. The pulse parameters were determined as follows E_1=−1.35 V, t_1=0.1 s, and E_2=−0.70 V, t_2=10 s (Scheme 1).

A bare glassy carbon electrode was modified with PPy nanofibers (PPy/GCE) following the same method for comparisons purposes.

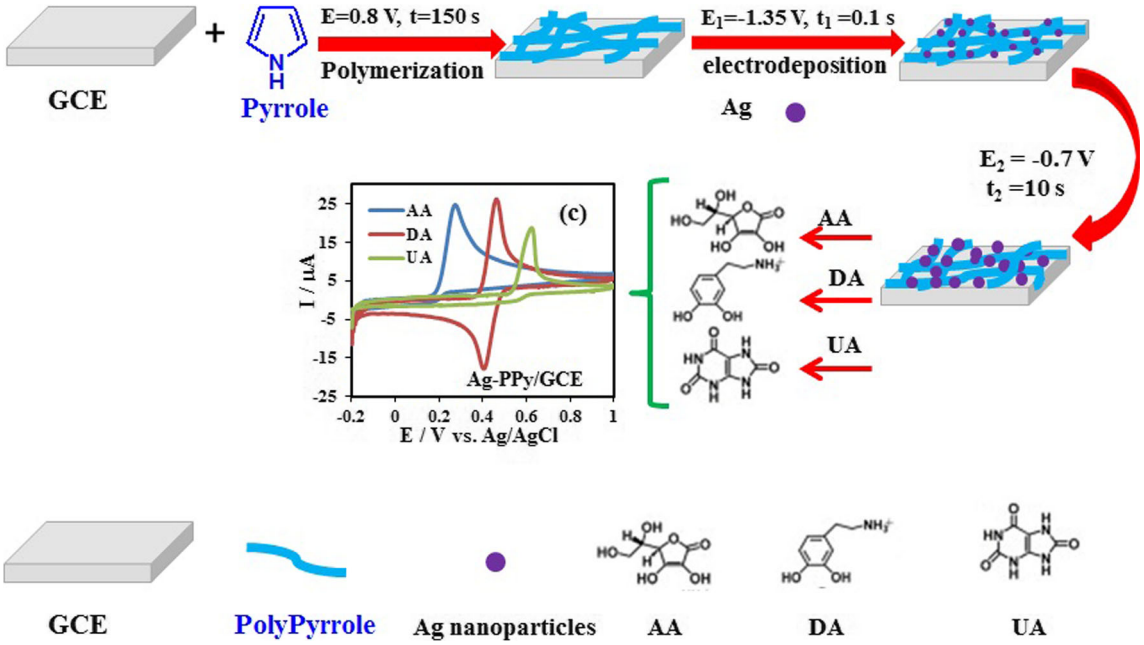

Scheme 1 Steps for preparation of Ag/PPy/glassy carbon modified electrode

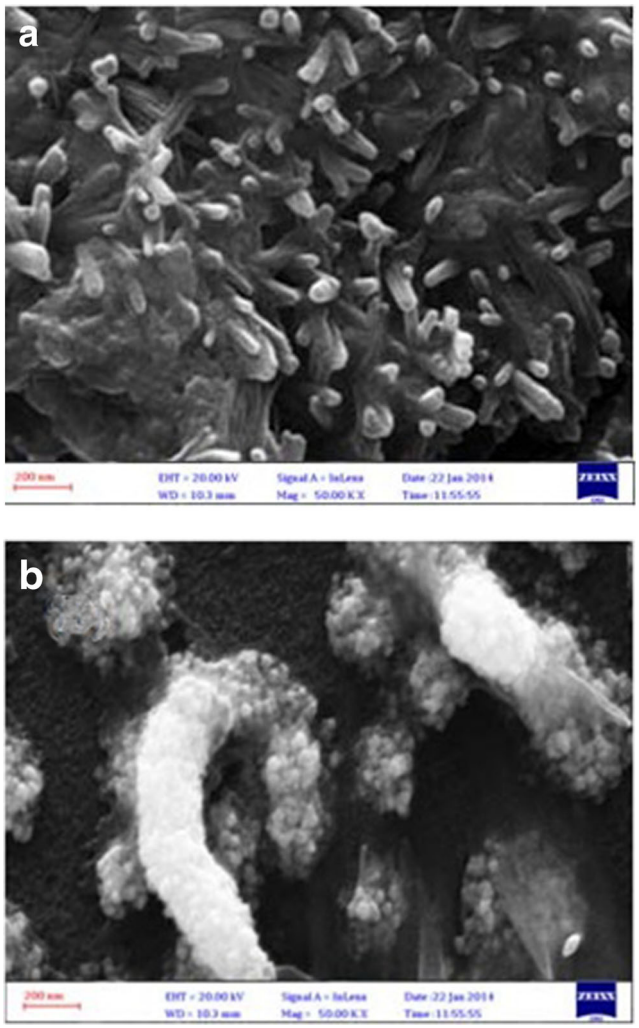

Fig. 1 FE-SEM pictures of PPy (**a**) and Ag/PPy (**b**)

Results and discussion

Characterization of the Ag-PPy/ GCE

Surface morphologies of the unmodified PPy nanofiber matrix and the Ag/PPy were characterized by FE-SEM. Figure 1a shows unmodified PPy nanofibers that are clean and relatively smooth in diameter of about 100 nm. The PPy nanofiber film with a well-ordered polymer chain structure has very large surface-to-volume ratio, which is useful for the incorporation of Ag nanoparticles and transport of electrical carriers along one controllable direction. Moreover, small cross dimensions and lots of micropores surrounded by the nanofibers could modify incorporation of analytes. Figure 1b shows the morphology of the Ag/PPy nanocomposite, in which Ag nanoparticles are homogeneously attached on the surface and aligned along the PPy nanofibers uniformly. The average size of Ag nanoparticles is about 50 nm. The small size and homogeneous distribution of Ag nanoparticles bring about many advantageous properties such as large surface are, good catalysis, and large numbers of active sites, which are conductive to a modification in the stability and sensitivity of Ag-PPy/GCE into biomolecules oxidation.

The XRD patterns of pure PPy and Ag/PPy nanocomposite are shown in Fig. 2. The broad peak at 2θ value at 20–30° is due to amorphous nature of polypyrrole (Fig. 2a) [36, 37].

The sharp peaks at 2θ values 37°, 44.5°, 52° and 76.5° can be assigned to the face centered cubic (fcc) phase of silver (111), (200), (220) and (311),

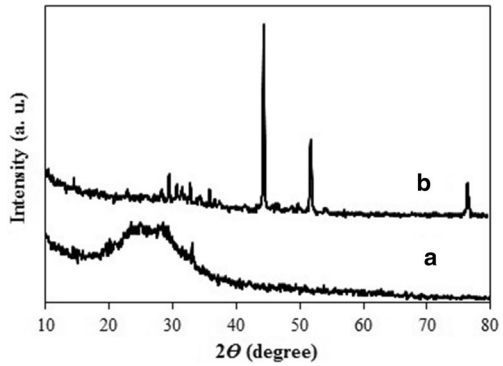

Fig. 2 XRD patterns of the PPy (curve **a**) and Ag/PPy (curve **b**)

respectively [38] and are in good agreement with the reported data (JCPDS File No. 04-0783). The existence of sharp peaks clearly indicates the presence of silver nanoparticles in the composites with their crystalline nature.

The interaction of polypyrrole and silver in PPy/Ag nanocomposite was evaluated by Fourier transform infrared (FT-IR) spectroscopy. Figure 3 shows the FT-IR spectra of the PPy and Ag/PPy nanocomposite. Figure 3a is correspond to PPy and the characteristic vibrational peaks for PPy are observed at 962 cm^{-1} (C-C out of plane vibration), 1,117 cm^{-1} (=C-H in plane vibration), 1,271 cm^{-1} (C-C), 1,461 cm^{-1} (pyrrole ring), 1,540 cm^{-1} (C = C), 1,709 cm^{-1} (C = N) and 3, 446 cm^{-1} (N-H stretching vibration) [21, 39].

Figure 3b shows the FT-IR spectra of Ag/PPy nanocomposite. The C-N stretching shifts from the higher wavenumber of 1,709 cm^{-1} for PPy to the lower wavenumber of 1,707 cm^{-1} for Ag/PPy and also N-H stretching shifts from the higher wavenumber of 3, 446 cm^{-1} for PPy to the lower wavenumber of 3, 423 cm^{-1} for Ag-PPy. These red shifts are attributed to the more delocalization of electrons at the nitrogen sites due to the interactions between Ag nanoparticles and PPy [40, 41].

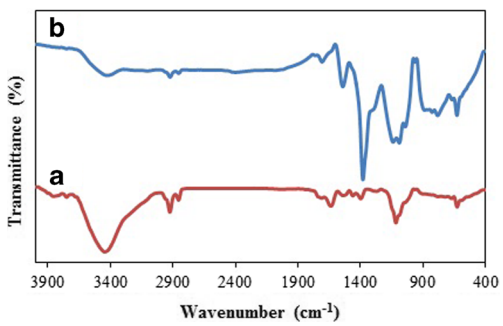

Fig. 3 FT-IR spectra of the PPy (curve **a**) and Ag/PPy (curve **b**)

Voltammetric responses of DA, UA, AA on the modified electrodes

The cyclic voltammetric responses of 200 μM AA, 40 μM DA, and 50 μM UA were recorded in 0.1 M Britton–Robinson buffer solution (BR) (Fig. 4). At the bare GCE (Fig. 4a), AA and UA show irreversible oxidation peaks at around 0.685 V and 0.680 V, respectively. DA showed a redox couple with the anodic peak at 0.57 V and cathodic peak at 0.3 V. As expected, it is very hard to recognize AA, DA and UA at the bare GCE as their oxidation peak potentials are very close. For PPy/GCE (Fig. 4b), the corresponding oxidation peak potentials of AA, DA and UA shifted to 0.44 V, 0.45 V, and 0.61 V, respectively. At the Ag-PPy/GCE, AA and UA showed well-defined oxidation peaks at 0.26 V and 0.6 V, respectively (Fig. 4c). For DA, a pair of redox peaks observed at 0.45 V and 0.42 V. Separation of anodic and cathodic peak potentials was 30 mV, which was much smaller than that on the bare GCE with a value of 270 mV. The oxidation peak currents of DA on the Ag-PPy/GCE was about four times higher than that on the bare GCE and is also larger than that of the PPy/GCE (3 times).

Moreover, the oxidation peak currents of AA and UA on the Ag-PPy/GCE increased about 2.5 times compared with that on the bare GCE. These values are larger than that of the PPy/GCE (about two times). The separation of the oxidation peak potentials at the Ag-PPy/GCE were 190 mV (AA and DA), 150 mV (DA and UA), and 340 mV (AA and UA). CV experiment results represented that Ag/PPy nanocomposites have high electrocatalytic activities toward the oxidation of these three species, which can be due to their unique structural features and excellent electrochemical properties.

The effect of solution pH value on the peak potential and current of AA, DA and UA was carefully investigated by CV in a larger pH range (pH 2.0–6.0). It can be seen from Fig. 5a that the peak current of AA, DA, and UA increased with increasing pH values until the pH reaches 4.0, the anodic peak current then decreased with further increase in the pH. The maximum anodic peak current was observed at pH 4.0. Figure 5b shows the effect of pH on the separation of peak potentials. All the peak potentials for the oxidation of AA, DA, and UA negatively shifted with higher pH value, indicating that protons take part in their electrode reaction processes. The maximum separation of peak potentials for AA-DA and DA-UA was observed at pH 4.0 and 4.5, respectively. In order to obtain high sensitivity and selectivity, pH 4.0 was selected as the optimal pH value for determination of AA, DA, and UA in their mixture.

Cyclic voltammograms with different scan rates in the range of 10–100 mV/s at the Ag-PPy/GCE are shown in Fig. 6a for AA, for DA in Fig. 6b, and for UA in Fig. 6c.

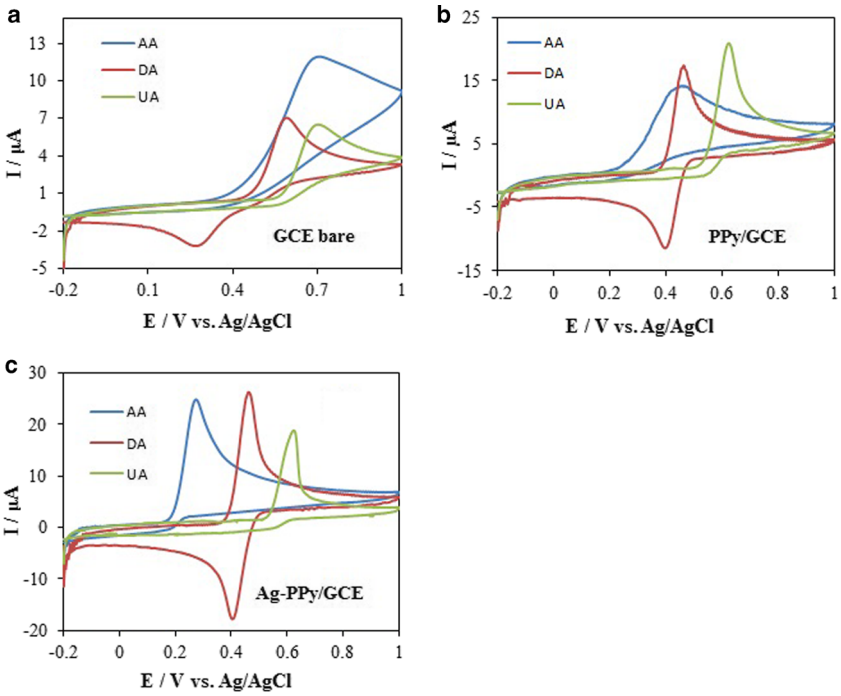

Fig. 4 Cyclic voltammograms of the 500 µM AA, 100 µM DA and 100.0 µM UA at the bare GCE (**a**), PPy/GCE (**b**) and Ag-PPy/GCE (**c**) in 0.1 M BR (pH 4.0) at a scan rate of 100 mV s^{-1}

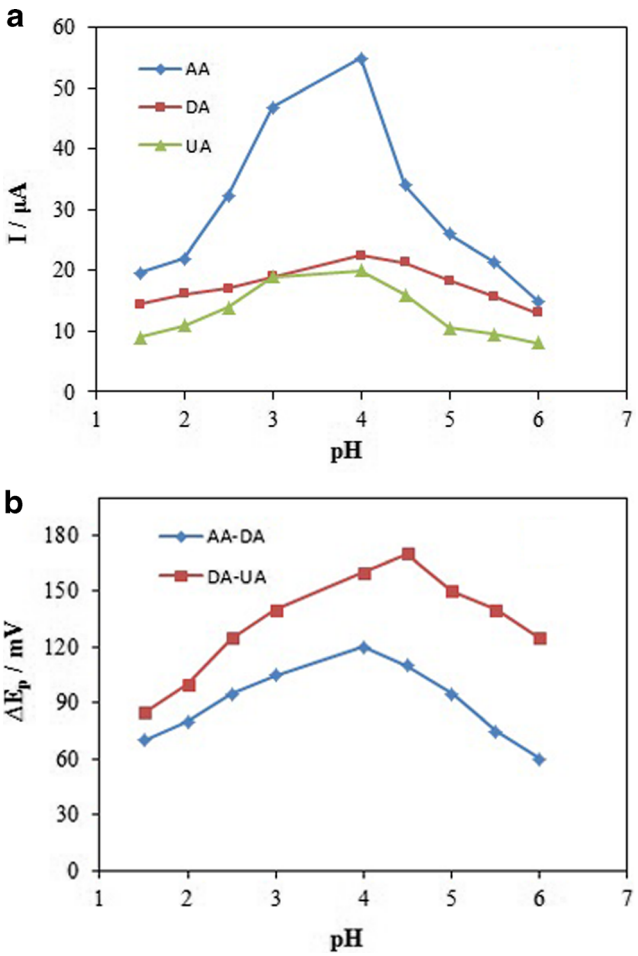

Fig. 5 The effects of pH on (**a**) the oxidation peak current of 1.0 mM AA, 0.1 mM DA, and 0.1 mM UA, (**b**) the oxidation peak potential of 1.0 mM AA, 0.1 mM DA and 0.1 mM UA in 0.1 M BR (pH 4.0) at a scan rate of 100 mV s^{-1}

The peak currents showed a linear relationship with square root of the scan rate (Insets in Fig. 6), indicating the diffusion controlled process dominated for AA, DA, and UA, because of the fast electron transfer rate on Ag-PPy/GCE.

Simultaneous determination of AA, DA and UA

CV responses of the mixture of AA, DA, and UA at bare GCE, PPy/GCE and Ag-PPy/GCE are shown in Fig. 7. At the bare GCE, the oxidation peaks of AA, DA, and UA completely overlap and show a broad peak at about 0.44 V. In contrast, at PPy/GCE, the overlapped voltammetric peak was resolved into three peaks at about 0.33 V, 0.45 V and 0.62 V, respectively. At the Ag-PPy/GCE, well-defined peaks of AA, DA, and UA appeared at 0.32 V, 0.45 V, and 0.61 V, respectively. The oxidation peak currents of AA, DA, and UA on the Ag-PPy/GCE are about two times higher than that on the bare GCE and PPy/GCE. Separation of the oxidation peak potentials for AA-DA, DA-UA, and AA-UA were about 120 mV, 170 mV and 290 mV, respectively, which is large enough to determine AA, DA and UA individually or simultaneously.

Determination of AA, DA, and UA in their mixtures was performed by application the DPV technique at the surface of Ag-PPy/GCE. In the experiments performed, concentration of one component was continuously increased with the successive addition of the standard sample solution, while concentrations of the other two species kept constant. As illustrated in Fig. 8a, by

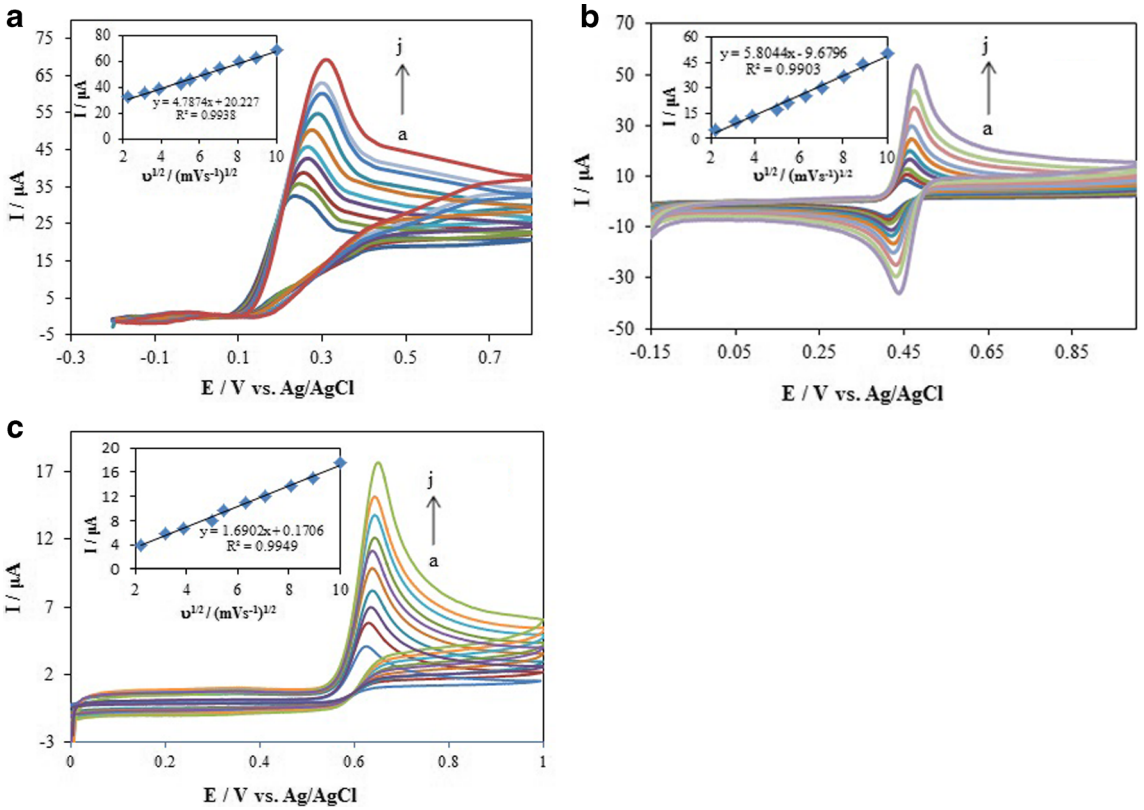

Fig. 6 Cyclic voltammograms of the Ag-PPy/GCE in 0.1 M RBS (pH 4.0) containing: (**a**) 5.0 mM AA, (**b**) 1.0 mM DA and (**c**) 0.1 mM UA at different scan rates (along the direction of *arrow*): 10, 20, 30, 40, 50, 60, 70, 80, 90, 100 mV s^{-1}. Insets show the plots of the peak current to the square root of the scan rates

increasing the AA concentration in the presence of 10 μM DA and 10 μM UA, the anodic peak currents of AA linearly increased ranging from 10 to 580 μM. Similar trends were observed by increasing the DA concentrations from 0.5 to 155 μM (Fig. 8b) in the solution containing 10 μM AA and 10 μM UA. Also, with the increase in the UA concentration in the presence of 10 μM AA and 10 μM DA, the anodic peak currents of UA linearly increased ranging from 2 to 100 μM (Fig. 8c). The detection limits for AA, DA, and UA were checked to be about 1.8, 0.1 and 0.5 μM at three folds of the signal-to-noise ratio (S/N=3), respectively. Thus, it is feasible to conclude that there is little interference of the other analytes in the mixture.

In comparison with previously developed modified electrodes, the proposed electrode exhibits better analytical performance (Table 1).

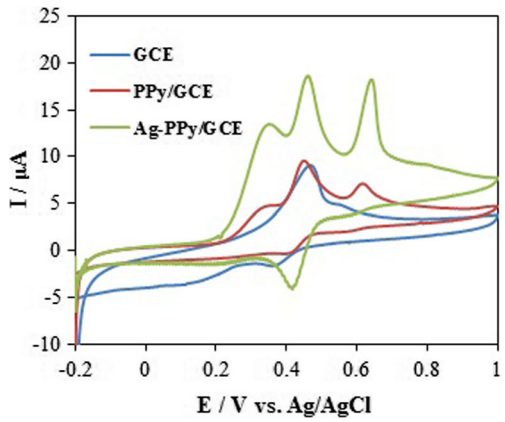

Fig. 7 CVs of mixture of 100 μM AA, 50 μM DA and 50 μM UA in 0.1 M BR (pH 4.0) at different electrodes. Scan rate: 25 mV/s

Interferences and reproducibility

The possible interference of some inorganic ions was evaluated by CV. It is found that 100-fold K^+, Na^+, Ca^{2+}, Mg^{2+}, Zn^{2+}, NH_4^+, Cl^-, NO_3^-, SO_4^{2-} and HCO_3^- do not interfere with the determination (signal change below 5%), represent the suggested electrode has excellent selectivity.

The reproducibility of Ag-PPy/GCE was investigated by determination of the response to the mixture solution of 0.5 mM AA, 50 μM DA, and 50 μM UA with five electrodes prepared under the same condition. The relative standard deviations (RSD) were 2.5 %, 1.6 %, and 2.3 % for AA, DA, and UA, respectively. Moreover, the

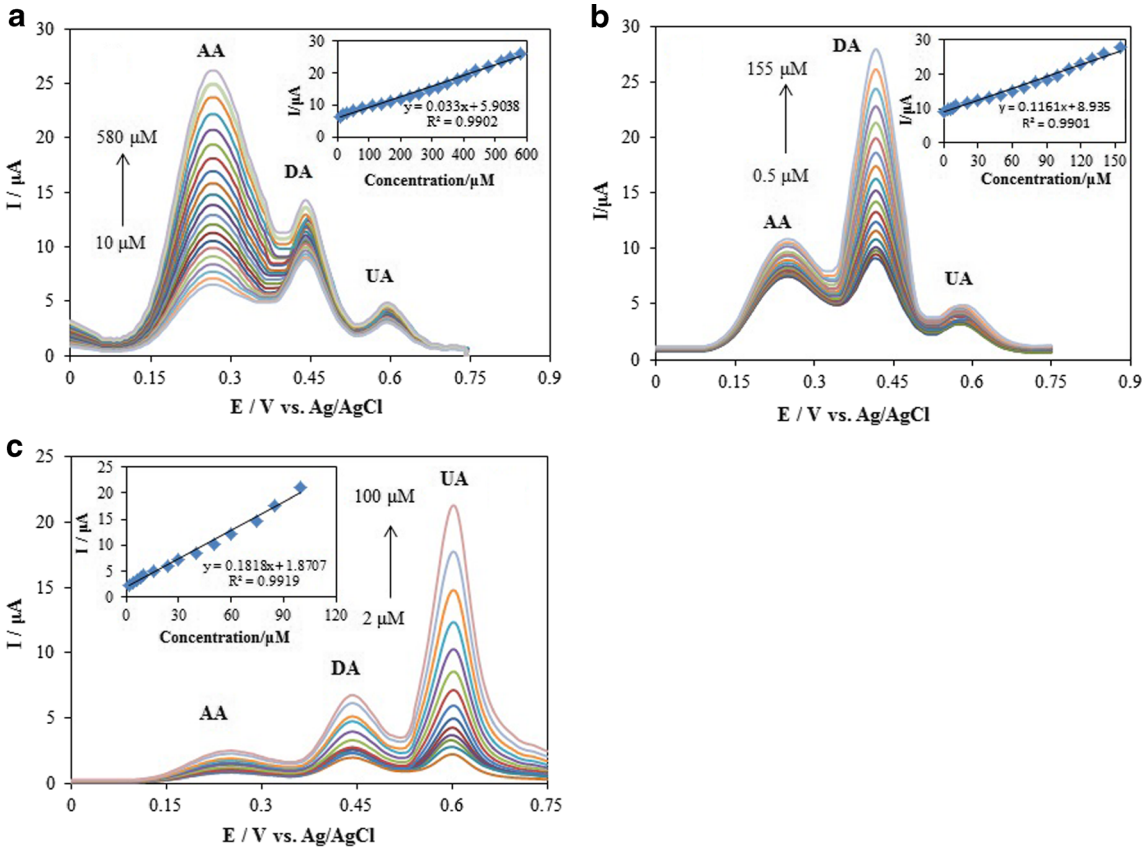

Fig. 8 DPVs at the Ag-PPy/GCE in 0.1 M BR (pH 4.0). **a**) 10 µM DA, 10 µM UA and different concentrations of AA; **b**) 10 µM AA, 10 µM UA and different concentrations of DA; **c**) 10 µM AA, 10 µM DA and different concentrations of UA. Scan rate: 25 mV/s pulse amplitude 25 mV. Inset: Plot of peak current vs. sample concentrations

stability of Ag-PPy/GCE was an important factor to be considered. Before the experiment, the modified electrode was stored at the room temperature for 30 days. The peak current intensity of AA, DA, and UA decayed by 4.3 %, 3.2 %, and 3.8 %, respectively; indicating a storage stability of the electrode.

Sample analysis

Determination of DA in dopamine hydrochloride injection

To verify the method reliability for analysis of DA in pharmaceutical products, Ag-PPy/GCE was applied to determine DA

Table 1 Comparison for the simultaneous determinations of AA, DA and UA at different modified electrodes

Electrode	Technique	Linear range (µM)		Detection limit (µM)				Ref.
		AA	DA	UA	AA	DA	UA	
Ag/CNT-CPE[a]	DPV	30–2000	0.8–64	–	12	0.3	–	[20]
ERGO/GCE[b]	DPV	500–2000	0.5–60	0.5–60	250	0.5	0.5	[42]
Ni NPs@Poly1,5-DAN/GCE[c]	SWV	100–500	100–500	–	0.01	0.011	–	[43]
Silver hexacyanoferrate NPs/CNT/GCE	DPV	4–78	2.4–130	2–150	0.42	0.14	0.06	[44]
Sol–gel /composite containing copper and MPS[d]	Amperometry	16–5000	7.3–2200	–	8.6	5.8	–	[45]
GNP/LC/GCE[e]	DPV	1–2500	0.06–85	–	0.3	0.02	–	[46]
Au/PTCA-Cys[f]	DPV	20–700	2–402	0.4–252.4	640	0.67	0.12	[47]
Ag-PLV[g]	DPV	0.3–10	0.5–10	10–1000	0.08	0.08	3.0	[48]
Ag-PPy/GCE	DPV	10–580	0.5–155	2–100	1.8	0.1	0.5	This work

[a] *CNT-CPE* Carbon nanotube-Carbon paste electrode; [b] *ERGO/GCE* Electrochemically reduced graphene oxide/Glassy carbon electrode; [c] *Ni NPs@Poly1,5-DAN/GCE* Nickel nanoparticles@Poly1,5-diaminonaphthalene/ Glassy carbon electrode; [d] *MPS* (3-Mercaptopropyl)trimethoysilane; [e] *GNP/LC* Gold nanoparticles/L-Cysteine; [f] Gold nanocrystal/3,4,9,10-perylenetetracarboxylic acid-L-Cysteine; [g] Silver-Poly(L-Valine)

Table 2 Determination of DA in dopamine hydrochloride injection (n=6)

DA specified (μM)	Added (μM)	Found (μM)	R.S.D. (%)	Recovery (%)
20	0	20.18	1.25	–
20	5	24.92	0.86	99.7
20	10	30.12	1.04	100.4
20	20	41.04	2.56	102.6
20	30	49.40	2.07	98.8
20	40	58.32	1.96	97.2

in dopamine hydrochloride injection (10 mg ml^{-1}). To this end, convenient amounts of the diluted sample were transferred into the electrochemical cell for determination using DPV. The analytical results are summarized in Table 2. The recovery ranged from 97.2 % to 102.6 %. The RSD (n=6) was less than 3.0 %. The results are acceptable; showing that the suggested method could be effectively used for determination of DA in commercial samples.

Determination of UA in human urine samples

Utilization of the proposed method in real sample analysis was also evaluated by direct analysis of UA in human urine samples. All the urine samples were diluted 100 times with BR (pH 4.0) before measurement. No other pretreatment process was performed. The standard addition method was used to evaluate the recovery. The recovery rates of the added samples ranged between 98.6 % and 100.8 % (Table 3); indicating the detection procedures are free from interferences of the urine sample matrix.

Conclusions

In summary, Ag/PPy nanocomposites were applied for the modification of GCE. This modified electrode exhibited high electrocatalytic activities towards the oxidation of AA, DA, and UA significantly decreasing their oxidation overpotentials and enhancing the peak currents. Large peak separation between these species could be obtained by DPV, indicating that the Ag-PPy/GCE facilitated their simultaneous determination. This electrochemical sensor showed excellent selectivity and sensitivity.

Table 3 Determination of UA in human urine samples (n=8)

Urine sample	Detected (μM)	Added (μM)	Found (μM)	Recovery (%)
1	29.54	25	54.43	99.8
2	31.66	25	55.87	98.6
3	19.53	25	44.90	100.8

Acknowledgments The authors gratefully acknowledge from the Research Council of Alzahra University and National Elites Fundation (Iran) for financial support to our research group.

References

1. Shi W, Liu C, Song Y, Lin N, Zhou S, Cai X (2012) An ascorbic acid amperometric sensor using over-oxidized polypyrrole and palladium nanoparticles composites. Biosens Bioeletron 38:100–106
2. Zhang X, Cao Y, Yu S, Yang E, Xi P (2013) An electrochemical biosensor for ascorbic acid based on carbon-supported PdNi nanoparticles. Biosens Bioeletron 44:183–190
3. Zeng Y, Zhou Y, Kong L, Zhou T, Shi G (2013) A novel composite of SiO_2-coated graphene oxide and molecularly imprinted polymers for electrochemical sensing dopamine. Biosens Bioeletron 45:25–33
4. Ulubay S, Dursun Z (2010) Cu nanoparticles incorporated polypyrrole modified GCE for sensitive simultaneous determination of dopamine and uric acid. Talanta 80:1461–1466
5. Benes FM (2001) Carlsson and the discovery of dopamine. Trends Pharmacol Sci 22:46–47
6. Huang S, Liao H, Chen D (2010) Simultaneous determination of norepinephrine, uric acid, and ascorbic acid at a screen printed carbon electrode modified with polyacrylic acid-coated multi-wall carbon nanotubes. Biosens Bioeletron 25:2351–2355
7. Lakshmi D, Whitcombe MJ, Davis F, Sharma PS, Prasad BB (2011) Electrochemical detection of uric acid in mixed and clinical samples. Electroanalysis 23:305–320
8. Culleton BF, Larson MG, Kannel WB, Levy D (1999) Serum uric acid and risk for cardiovascular disease and death: the Framingham Heart Study. Ann Intern Med 131:7–13
9. Vulcu A, Grosan C, Muresan LM, Pruneanu S, Olenic L (2013) Modified gold electrodes based on thiocytosine/guanine-gold nanoparticles for uric and ascorbic acid determination. Electrochim Acta 88:839–846
10. Hirsch E, Graybiel AM, Agid YA (1988) Melanized dopaminergic neurons are differentially susceptible to degeneration in Parkinson's disease. Nature 334:345–348
11. Wightman RM, May LJ, Michael AC (1988) Detection of dopamine dynamics in the brain. Anal Chem 60:769A–793A
12. Chih YK, Yang MC (2013) An 2,2′-azino-bis(3-ethylbenzthiazoline-6-sulfonic acid)-immobilized electrode for the simultaneous detection of dopamine and uric acid in the presence of ascorbic acid. Bioelectrochem 91:44–51
13. Sun CL, Lee HH, Yang JM, Wu CC (2011) The simultaneous electrochemical detection of ascorbic acid, dopamine, and uric acid using graphene/size-selected Pt nanocomposites. Biosens Bioeletron 26:3450–3455
14. Gopalan AI, Lee KP, Manesh KM, Santhosh P, Kim JH, Kang JS (2007) Electrochemical determination of dopamine and ascorbic acid at a novel gold nanoparticles distributed poly(4-aminothiophenol) modified electrode. Talanta 71:1774–1781
15. Safavi A, Moradlou O, Tajabadi F (2006) Simultaneous determination of dopamine, ascorbic acid, and uric acid ysing carbon ionic liquid electrode. Anal Biochem 359:224–229
16. Wu J, Suls J, Sansen W (2000) Amperometric determination of ascorbic acid on screen-printing ruthenium dioxide electrode. Electrochem Commun 2:90–93
17. Yang YJ, Li W (2014) CTAB functionalized graphene oxide/multiwalled carbon nanotube composite modified electrode for

the simultaneous determination of ascorbic acid, dopamine, uric acid and nitrite. Biosens Bioeletron 56:300–306
18. Li Y, Du J, Yang J, Liu D, Lu X (2012) Electrocatalytic detection of dopamine in the presence of ascorbic acid and uric acid using single-walled carbon nanotubes modified electrode. Colloids Surf B Biointerfaces 97:32–36
19. Ahmar H, Fakhari AR, Nabid MR, Tabatabaei Rezaei SJ, Bide Y (2012) Electrocatalytic oxidation of oxalic acid on palladium nanoparticles encapsulated on polyamidoamine dendrimer-grafted multi-walled carbon nanotubes hybrid material. Sens Actuators B 171–172:611–618
20. Tashkhourian J, Hormozi Nezhad MR, Khodavesi J, Javadi S (2009) Silver nanoparticles modified carbon nanotube paste electrode for simultaneous determination of dopamine and ascorbic acid. J Electroanal Chem 633:85–91
21. Berdre MD, Basavaraja S, Deshpande R, Balaji DS, Venkataraman A (2010) Preparation and characterization of polypyrrole silver nanocomposites via interfacial polymerization. Int J Polymer Mater 59:531–543
22. Ghanbari K (2014) Fabrication of silver nanoparticles–polypyrrole composite modified electrode for electrocatalytic oxidation of hydrazine. Synth Met 195:234–240
23. Chen C, Chiu M, Sheu J, Wei K (2008) Photoresponses and memory effects in organic thin film transistors incorporating poly(3-hexylthiophene)/CdSe quantum dots. Appl Phys Lett 92:143105-1–143105-3
24. Chiu M, Chen C, Sheu J, Wei K (2009) An optical programming/electrical erasing memory device: organic thin film transistors incorporating core/shell CdSe@ZnSe quantum dots and poly(3-hexylthiophene). Org Electron 10:769–774
25. Chen X, Parker SG, Zou G, Su W, Zhang Q (2010) β-cyclodextrin-functionalized silver nanoparticles for the naked eye detection of aromatic isomers. ACS Nano 4:6387–6394
26. Liu CJ, Burghaus U, Besenbacher F, Wang ZL (2010) Preparation and characterization of nanomaterials for sustainable energy production. ACS Nano 4:5517–5526
27. Zeng Q, Jiang X, Yu A, Lu G (2007) Growth mechanisms of silver nanoparticles: a molecular dynamics study. Nanotechnology 18: 035708–035714
28. Jin R, Cao YC, Hao E, Metraux GS, Schatz GC, MirKin CA (2003) Controlling anisotropic nanoparticle growth through plasmon excitation. Nature 425:487–490
29. Severin N, Kirstein S, Sokolov SM, Rabe JP (2009) Rapid trench channeling of graphenes with catalytic silver nanoparticles. Nano Lett 9:457–461
30. Davarpanah J, Kiasat AR (2013) Catalytic application of silver nanoparticles immobilized to rice husk-SiO_2-aminopropylsilane composite as recyclable catalyst in the aqueous reduction of nitroarenes. Catal Commun 41:6–11
31. Panacek A, Kvitek L, Prucek R, Kolar M, Vecerova R, Pizurova N et al (2006) Silver colloid nanoparticles: synthesis, characterization, and their antibacterial activity. J Phys Chem B 110:16248–16253
32. Ajitha B, Ashok Kumar Reddy Y, Sreedhara Reddy P (2015) Enhanced antimicrobial activity of silver nanoparticles with controlled particle size by pH variation. Powder Technol 269:110–117
33. Zeng R, Rong MZ, Zhang MQ, Liang HC, Zeng HM (2002) Laser ablation of polymer-based silver nanocomposites. Appl Surf Sci 187:239–247
34. Ustarroz J, Gupta U, Hubin A, Bals S, Terryn H (2010) Electrodeposition of Ag nanoparticles onto carbon coated TEM grids: a direct approach to study early stages of nucleation. Electrochem Commun 12:1706–1709
35. Rezaei B, Khalili Boroujeni M, Ensafi AA (2014) A novel electrochemical nanocomposite imprinted sensor for the determination of lorazepam based on modified polypyrrole@sol–gel@gold nanoparticles/pencil graphite electrode. Electrochim Acta 123: 332–339
36. Allena NS, Murray KS, Fleming RJ, Saunders BR (1997) Physical properties of polypyrrole films containing trisoxalatometallate anions and prepared from aqueous solution. Synth Met 87:237–247
37. Tambolia MS, Kulkarni MV, Patil RH, Gade WN, Navale SC, Kale BB (2012) Nanowires of silver–polyaniline nanocomposite synthesized via in situ polymerization and its novel functionality as an antibacterial agent. Colloids Surf B Biointerfaces 92:35–41
38. Chen C, Wang L, Jiang G, Zhou J, Chen X, Yu H (2006) Study on the synthesis of silver nanowires with adjustable diameters through the polyol process. Nanotechnology 17:3933–3938
39. Ye D, Luo L, Ding Y, Chen Q, Liu X (2011) A novel nitrite sensor based on graphene/polypyrrole/chitosan nanocomposite modified glassy carbon electrode. Analyst 136:4563–4569
40. Yang X, Li L, Shang S, Pan G, Yu X, Yan G (2010) Facial synthesis of polypyrrole/silver nanocomposites at the water/ionic liquid interface and their electrochemical properties. Mat Lett 64:1918–1920
41. Babu K, Dhandapani P, Maruthamuthu S, Kulandainathan MA (2012) One pot synthesis of polypyrrole silver nanocomposite on cotton fabrics for multifunctional property. Carbohydr Polym 90: 1557–1563
42. Yang L, Liu D, Hung J, You T (2014) Simultaneous determination of dopamine, ascorbic acid and uric acid at electrochemically reduced graphene oxide midiied electrode. Sens Actuators B 193: 166–172
43. Hathoot AA, Yousef US, Shatla AS, Abdel-Azzem M (2012) Voltammetric simultaneous determination of glucose, ascorbic acid and dopamine on glassy carbon electrode modified by NiNPs@poly 1,5-diaminonaphthalene. Electrochim Acta 85:531–537
44. Noroozifar M, Khorasani-Motlagh M, Taheri A (2010) Preparation of silver hexacyanoferratenanoparticles and its application for the simultaneous determination of ascorbic acid, dopamine and uric acid. Talanta 80:1657–1664
45. Shankaran DR, Limura K, Kato T (2003) Simultaneous determination of ascorbic acid and dopamine at a sol–gel composite electrode. Sens Actuators B 94:73–80
46. Hu G, Guo Y, Shao S (2009) Simultaneous determination of dopamine and ascorbic acid using the Nano-gold self-assembled glassy carbon electrode. Electroanalysis 21:1200–1206
47. Zhang W, Chai Y, Yuan R, Han J, Chen S (2013) Deposited gold nanocrystals enhanced porous PTCA-Cys layer for simultaneous detection of ascorbic acid, dopamine and uric acid. Sens Actuators B 183:157–162
48. Hu W, Sun D, Ma W (2010) Silver doped poly(L-valine) modified glassy carbon electrode for the simultaneous determination of uric acid, ascorbic acid and dopamine. Electroanalysis 22:584–589